JOURNAL OF SPACECRAFT AND ROCKETS
Vol. 44, No. 3, May–June 2007

Finite Element Modeling of Sail Deformation Under Solar Radiation Pressure

Hiraku Sakamoto*
University of Colorado at Boulder, Boulder, Colorado 80309-0429
Yasuyuki Miyazaki†
Nihon University, Chiba 274-8501, Japan
and
K. C. Park‡
University of Colorado at Boulder, Boulder, Colorado 80309-0429

DOI: 10.2514/1.23474

A numerical structural model of a thin-film sail that simulates the deformation caused by solar-radiation pressure is developed, using a geometrically nonlinear finite element method (FEM). By using the finite element presented in this study, the force and moment exerted on an arbitrarily shaped solar sail subjected to solar pressure can be calculated accurately. In addition, it is shown that the sail deformation due to a solar-pressure load can be approximated by the deformation caused by the corresponding uniform gas-pressure load. This finding will significantly simplify analyses to improve attitude controller design as well as structural design of sailcraft, because commercially available FEM software can be used for the analyses.

Nomenclature

A	=	sail surface domain
A_e	=	area of an element
a_1 a_2, a_3	=	sail optical coefficients
B_f, B_b	=	sail non-Lambertian coefficients of front and back surfaces
E_m	=	Young's modulus of membrane
e_f, e_b	=	sail emissivities of front and back surfaces
e_{ij}	=	component of Green's strain tensor
$\boldsymbol{f}$, $\hat{\boldsymbol{f}}$	=	total solar-radiation force vector exerted on sail, and its normalized unit vector
$\boldsymbol{f}_i$	=	nodal solar-radiation force vector of ith node
$\boldsymbol{g}_1$, $\boldsymbol{g}_2$	=	covariant base vectors
h_m	=	sail-membrane thickness
$\boldsymbol{I}$	=	identity matrix
$\boldsymbol{J}^{(m)}$	=	tensors defined in Eq. (22), $m = 1, 2, 3$
$J_i^{(1)}$, $J_{ij}^{(2)}$, $J_{ijk}^{(3)}$	=	components of tensor $\boldsymbol{J}^{(m)}$
$\boldsymbol{K}^{(m)}$	=	tensors defined in Eq. (23), $m = 1, 2, 3$
$K_i^{(1)}$, $K_{ij}^{(2)}$, $K_{ij}^{(3)}$	=	components of tensor $\boldsymbol{K}^{(m)}$
ℓ	=	membrane length with initial prestrain ε_0
ℓ_0	=	undeformed membrane length
$\boldsymbol{m}$, m_2	=	total moment vector at the coordinate origin, and its y_2 component
$\boldsymbol{m}_m$	=	total moment with respect to the center of mass of entire sailcraft
m_t	=	total mass of sail membrane
N_i	=	shape function for ith node
$\boldsymbol{n}$, $\hat{\boldsymbol{n}}$	=	surface normal vector and its unit vector
n_n	=	number of nodes in element
$\hat{\boldsymbol{n}}_0$	=	unit normal vector of undeformed sail reference surface
$P(r_s)$	=	solar pressure on flat surface, normal to the sun at a distance r_s from the sun
p	=	uniform gas-pressure magnitude
$\boldsymbol{p}$	=	solar-radiation force vector defined in Eqs. (8) and (9)
p_1, p_2	=	Gauss integration points in local coordinate
R	=	radius of circular sail
r	=	radius of curvature of deformed membrane
$\boldsymbol{r}_m$	=	position vector of center of mass of sail membrane
$\boldsymbol{r}_m^t$	=	position vector of center of mass of entire sailcraft
$\boldsymbol{r}_p$, r_{p1}	=	position vector of center of pressure, and its y_1 component
r_s	=	distance from the sun
$\hat{\boldsymbol{r}}_0$	=	unit sun–photon incidence vector
s	=	sail specular reflectivity
T	=	uniform tension in y_1-direction in membrane per unit width
$\hat{\boldsymbol{t}}$	=	unit surface tangent vector, which is on the same plane with $\hat{\boldsymbol{n}}$ and $\hat{\boldsymbol{r}}_0$
u_i	=	displacement of the membrane in the y_i-direction
w	=	weight function of Gaussian integral points $(\xi_1, \xi_2) = (p_1, p_2)$
$\boldsymbol{x}$	=	position vector
$\boldsymbol{x}_i$	=	nodal position vector of ith node
(y_1, y_2, y_3)	=	Cartesian coordinate
α	=	angle between sun–photon incidence direction and surface normal of deformed sail
α_0	=	angle between sun–photon incidence direction and surface normal of reference surface (pitch angle)
β	=	sign of $(\hat{\boldsymbol{n}} \cdot \hat{\boldsymbol{r}}_0)$
γ	=	edge slope of circular sail
ε	=	membrane nominal strain
ε_d	=	membrane strain due to deformation
ε_0	=	initial uniform biaxial prestrain in membrane
κ	=	arbitrary scalar
λ	=	scale factor defined in Eq. (27)
ν	=	Poisson's ratio of membrane

Received 25 February 2006; revision received 3 September 2006; accepted for publication 12 October 2006.

*JSPS Postdoctoral Fellow, Center for Aerospace Structures, UCB 429; hiraku.sakamoto@colorado.edu. Member AIAA.

†Associate Professor, Department of Aerospace Engineering, College of Science and Technology, 7-24-1 Narashinodai, Funabashi.

‡Professor, Center for Aerospace Structures and Department of Aerospace Engineering Sciences, UCB 429. Associate Fellow AIAA.

(ξ_1, ξ_2) = local coordinate
ρ = sail reflectivity
ρ_m = sail-membrane density
σ_{ij} = component of second Piola–Kirchhoff stress tensor
σ_m = prestress in sail membrane
ϕ = centerline angle between sail reference normal vector and force vector
ψ = central angle for deformed membrane arc

Introduction

ATTITUDE and navigation control systems for solar sails have been widely studied, yet most analyses to date assume that the sail is always flat. An actual sail in orbit, however, billows out due to solar-radiation pressure. Such deformation of the sail affects the resultant thrust-force vector exerted on the sail and modifies the resultant moment acting on the sail because the center-of-pressure (cp) location and the center-of-mass (cm) location are moved, as illustrated in Fig. 1. It is desired to predict these changes of force and torque vectors as precisely as possible using a billowed sail model for the following three reasons. First, such a model clarifies the effects of structural design parameters, e.g., sail shape, sail prestress level, etc., on the thrust force and the cp-to-cm offset torque on the sail. These relations determine the requirement for control devices, and knowing the parameter dependencies between the structures and the control system enables simultaneous optimization of both designs. Second, a billowed-sail force/torque model can be used to develop appropriate attitude and navigation control algorithms because it enables high-fidelity dynamic simulations. Third, the precise prediction of the cp and cm locations enables new attitude control methods for sailcraft. Among various attitude control methods proposed to date, the prevailing approach is to change a cp location and/or a cm location of the sail [1–3]. These methods are preferred because the cp-to-cm offset torque is relatively large to be counteracted by conventional reaction wheels [4]. However, these methods require an accurate knowledge of current cp/cm locations to realize an efficient and robust control; thus, an accurate force/torque model is needed. To this end, the present study aims at developing a sail model that can predict the force/torque vectors exerted on the deformed sail under the action of solar pressure. A geometrically nonlinear finite element method (FEM) is employed in this study.

Wright [5] and McInnes [6] present a parametric force model for simple sail geometries (a square sail and a heliogyro sail) allowing for sail billow. These models were developed during the Jet Propulsion Laboratory (JPL) comet Halley rendezvous study. Mengali and Quarta [7] used this JPL model to develop a navigation control algorithm. Rios-Reyes and Scheeres [8] provided analytical solutions for the force and moment exerted on a sail with prescribed curvatures. This analytical approach, however, can be used only for simple sail geometries, such as a circular sail with a fixed edge. Wie et al. [2–4] modeled the torque caused by a cp-to-cm offset in an attitude-dynamics simulation for sailcraft where the cp-to-cm offset was simply fixed at a given value. All the previous studies described herein used largely simplified sail models to predict force/torque vectors on the sail by assuming simple sail shapes, fixed sail boundary conditions, uniform prestress throughout the sail, or fixed cp-to-cm offsets. Practical sailcraft, on the contrary, will have various sail shapes, various sail boundary conditions, and various prestress distributions. Some researchers even discuss spin-stabilized sailcraft, whose sail will be subject to distributed centrifugal load [9]. The prediction of the force and torque vectors exerted on these more practical sail configurations under the action of solar pressure is not yet adequately addressed.

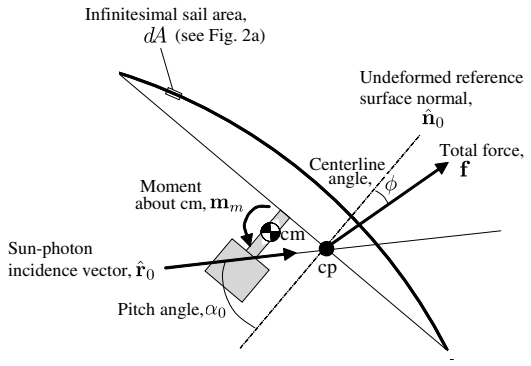

Fig. 1 Force, moment, center of pressure, and center of mass for a billowed solar sail.

To obtain the deformed sail shape caused by solar pressure, geometrical nonlinearity has to be properly taken into account. For example, the sail stiffness depends on prestress, and sail deformation causes a change in the distribution and magnitude of the membrane stresses acting in the sail. In addition, the direction of pressure force should change with the sail deflection. The recent development of a geometrically nonlinear FEM has made it possible to model the large deformations of prestressed membranes. Furthermore, the tension-field theory is widely used to allow for determining the effect of wrinkles on membrane behavior [10], and even transient dynamic analyses are possible [11]. Past studies on finite element modeling of membranes are summarized in [10]. Using FEM, various sail-shape models with various boundary conditions and with nonuniform prestress distributions can be constructed. Accordingly, this study develops a membrane finite element (FE), using a geometrically nonlinear FEM framework, that can calculate the force/torque exerted on the deformed sail FE model (step 1), and can compute the sail deformation caused by solar-radiation pressure (step 2).

To accomplish this objective, the paper first derives the general FE representation for a plane stress element that accounts for the effects of solar pressure. Then, an analytical solution of Rios-Reyes and Scheeres [8] is invoked for the special case of a billowed sail with a simple prescribed geometry, and a comparison with corresponding FE results is presented for a circular sail. This comparison verifies that the developed finite element accurately calculates the force/torque exerted on the deformed sail (step 1). Next, an analytical solution is derived for an infinite-width membrane with two fixed edges subjected to a uniform gas-pressure loading, and a comparison with corresponding FE results is presented. This solution is used to validate the uniform gas-pressure FE model. Then, the deformed shape caused by the gas pressure is compared to the one subjected to a solar-radiation pressure. By this comparison, it is observed that the solar-pressure model provides the physically valid deformed shape (step 2). An interesting finding here is that the corresponding uniform gas-pressure value is identified that can be used to approximate the solar-pressure effect on the membrane deformation. The assumptions underlying this gas-pressure approximation are presented. Because most of commercially available geometrically nonlinear FEM software is capable of gas-pressure modeling, this finding significantly facilitates analyses. Finally, a methodology to predict the force/torque on the deformed sail subjected to solar pressure is presented as a summary of the present work.

Finite Element Formulation

Overview

In this section, a membrane finite element under the action of solar pressure is formulated, and the cp/cm position vectors are derived. First, the vector representation of solar pressure is derived so that the pressure model is easily incorporated into the local coordinate system, which is commonly used in the geometrically nonlinear FE formulation. Second, the nodal force vector and the Jacobian of the nodal force vector, which gives a tangent stiffness matrix, are derived. Finally, forces and moments in each finite element are summed to find cp/cm locations of the entire sail FE model.

Vector Representation of Solar-Radiation Force

Following [6,8], the differential solar-radiation force acting on an infinitesimal membrane area, located by the position vector $\boldsymbol{x}$, may be written as

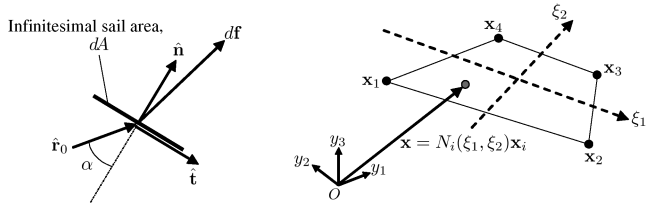

a) Vectors on an infinitesimal section of the sail **b) Membrane finite element (case of a 4-node quadrilateral)**

Fig. 2 Definitions of vectors in infinitesimal sail section and membrane finite element.

$$\mathrm{d}\boldsymbol{f} = P(r_s)[(a_1\cos^2\alpha + a_2\cos\alpha)\hat{\boldsymbol{n}}\beta + a_3\cos\alpha\sin\alpha\hat{\boldsymbol{t}}]\,\mathrm{d}A \quad (1)$$

where $a_1 = 1 + \rho s$, $a_2 = B_f(1-s)\rho + (1-\rho)(e_f B_f - e_b B_b)/(e_f + e_b)$, $a_3 = 1 - \rho s$, and $\beta = \mathrm{sgn}(\hat{\boldsymbol{n}}\cdot\hat{\boldsymbol{r}}_0)$. The relationship between the vectors in Eq. (1) is illustrated in Fig. 2a. Note that the angle α_0 in Fig. 1 is the sun–photon incidence angle with respect to the undeformed sail reference surface, whereas the angle α in Fig. 2a is the sun–photon incidence angle with respect to the deformed sail surface. Introducing β gives a freedom to define the normal vector in either direction perpendicular to the sail surface. Using the relations $\cos\alpha = |\hat{\boldsymbol{n}}\cdot\hat{\boldsymbol{r}}_0|$, $\sin\alpha = \| \hat{\boldsymbol{n}}\times(\hat{\boldsymbol{n}}\times\hat{\boldsymbol{r}}_0)\|$, and

$$\hat{\boldsymbol{t}} = -\frac{\hat{\boldsymbol{n}}\times(\hat{\boldsymbol{n}}\times\hat{\boldsymbol{r}}_0)}{\| \hat{\boldsymbol{n}}\times(\hat{\boldsymbol{n}}\times\hat{\boldsymbol{r}}_0)\|} \quad (2)$$

it follows that

$$\sin\alpha\hat{\boldsymbol{t}} = -\hat{\boldsymbol{n}}\times(\hat{\boldsymbol{n}}\times\hat{\boldsymbol{r}}_0) = -[(\hat{\boldsymbol{n}}\cdot\hat{\boldsymbol{r}}_0)\hat{\boldsymbol{n}} - \hat{\boldsymbol{r}}_0] \quad (3)$$

Consequently, Eq. (1) becomes

$$\mathrm{d}\boldsymbol{f} = P(r_s)|\hat{\boldsymbol{n}}\cdot\hat{\boldsymbol{r}}_0|\{[(a_1 - a_3)\hat{\boldsymbol{n}}\cdot\hat{\boldsymbol{r}}_0 + a_2\beta]\hat{\boldsymbol{n}} + a_3\hat{\boldsymbol{r}}_0\}\,\mathrm{d}A \quad (4)$$

Nodal Force Vectors and Tangent Stiffness Matrix

In the following formulation, a local coordinate system (ξ_1, ξ_2) is used. An example case for a four-node quadrilateral membrane finite element is illustrated in Fig. 2b. This four-node element is used in the following analysis in this paper, though the formulation in this section can be applied to any kind of plane-stress elements. The surface normal vector for the element is given in terms of the local coordinates by

$$\hat{\boldsymbol{n}} = \frac{\boldsymbol{n}}{\|\boldsymbol{n}\|} \quad (5)$$

where

$$\boldsymbol{n} = \boldsymbol{g}_1\times\boldsymbol{g}_2 \quad (6)$$

with

$$\boldsymbol{g}_\alpha = \frac{\partial N_i}{\partial\xi_\alpha}\boldsymbol{x}_i \qquad (\alpha = 1,2 \quad \text{and} \quad i = 1,\cdots,n_n) \quad (7)$$

$(\boldsymbol{g}_1, \boldsymbol{g}_2)$ is a set of the covariant base vectors, which are tangent to the local coordinate axes. Note that repeated indices imply summation over the index range. In addition, $\mathrm{d}A = \|\boldsymbol{n}\|\,\mathrm{d}\xi_1\,\mathrm{d}\xi_2$. Substitution of Eq. (5) into Eq. (4) yields the differential force vector as a function of the local coordinates of the element; that is,

$$\mathrm{d}\boldsymbol{f} = (P(r_s)|\boldsymbol{n}\cdot\hat{\boldsymbol{r}}_0|\{[(a_1 - a_3)\hat{\boldsymbol{n}}\cdot\hat{\boldsymbol{r}}_0 + a_2\beta]\hat{\boldsymbol{n}} + a_3\hat{\boldsymbol{r}}_0\})\,\mathrm{d}\xi_1\,\mathrm{d}\xi_2 \quad (8)$$

$$\equiv \boldsymbol{p}(\xi_1,\xi_2)\,\mathrm{d}\xi_1\,\mathrm{d}\xi_2 \quad (9)$$

Gauss integration is employed to obtain an equivalent nodal force vector $\boldsymbol{f}_i$, given by

$$\boldsymbol{f}_i = \int_{A_e} N_i\,\mathrm{d}\boldsymbol{f} \quad (10)$$

$$\approx \sum_{p_1}\sum_{p_2} w(p_1,p_2)N_i(p_1,p_2)\boldsymbol{p}(p_1,p_2) \quad (11)$$

Furthermore, the following Jacobian is subtracted from the original tangent stiffness matrix without the effect of pressure forces:

$$\frac{\partial\boldsymbol{f}_i}{\partial\boldsymbol{x}_j} = \sum_{p_1}\sum_{p_2} w(p_1,p_2)N_i(p_1,p_2)\frac{\partial\boldsymbol{p}(p_1,p_2)}{\partial\boldsymbol{x}_j} \quad (12)$$

The explicit expression for $[\partial\boldsymbol{p}(\xi_1,\xi_2)/\partial\boldsymbol{x}_j]$ in Eq. (12) is shown in Appendix A. This Jacobian is subtracted because the tangent stiffness matrix is the Jacobian of internal nodal forces, whereas the pressure $\boldsymbol{f}_i$ is external.

Total Force, Total Moment, Center of Pressure, and Center of Mass

The total pressure force and moment acting on a sail are obtained by integrating $\mathrm{d}\boldsymbol{f}$ and $\mathrm{d}\boldsymbol{m} = \boldsymbol{x}\times\mathrm{d}\boldsymbol{f}$ over the entire sail area.

$$\boldsymbol{f} = \int_A \mathrm{d}\boldsymbol{f} \quad (13)$$

$$\approx \sum_e\left[\sum_{p_1}\sum_{p_2} w(p_1,p_2)\boldsymbol{p}(p_1,p_2)\right] \quad (14)$$

$$\boldsymbol{m} = \int_A \mathrm{d}\boldsymbol{m} \quad (15)$$

$$\approx \sum_e\left[\sum_{p_1}\sum_{p_2} w(p_1,p_2)[N_i(p_1,p_2)\boldsymbol{x}_i]\times\boldsymbol{p}(p_1,p_2)\right] \quad (16)$$

where $\sum_e$ stands for the sum of all the elements, and $i = 1,\cdots,n_n$. The cp location $\boldsymbol{r}_p$, relative to the coordinate frame in Fig. 2b, satisfies $\boldsymbol{m} = \boldsymbol{r}_p\times\boldsymbol{f}$ by definition. Thus,

$$\boldsymbol{r}_p = \bar{\boldsymbol{r}}_p + \kappa\hat{\boldsymbol{f}} \quad (17)$$

where

$$\bar{\boldsymbol{r}}_p = \frac{1}{\|\boldsymbol{f}\|^2}\boldsymbol{f}\times\boldsymbol{m} \quad (18)$$

with κ as an arbitrary scalar [8]. In other words, there exist an infinite number of cp locations along a line in the direction of the thrust force. In the present study, a value of κ is used that makes $\boldsymbol{r}_p$ a point on the undeformed flat sail reference plane. Next, the cm location of the overall membrane elements, relative to the coordinate frame in Fig. 2b, is given by

$$\boldsymbol{r}_m = \frac{1}{m_t}\int_A \rho_m h_m\boldsymbol{x}\,\mathrm{d}A \quad (19)$$

$$\approx \frac{1}{m_t}\sum_e\left[\sum_{p_1}\sum_{p_2} w(p_1,p_2)\rho_m h_m[N_i(p_1,p_2)\boldsymbol{x}_i]\|\boldsymbol{n}\|\right] \quad (20)$$

The cm location for an entire sailcraft $\boldsymbol{r}_m^t$ is computed adding the contributions from the masses of other components in the sailcraft. Once $\boldsymbol{r}_m^t$ is obtained, a moment acting on the sail in terms of the coordinate frame, $\boldsymbol{m}$, can be transformed to a moment in terms of the cm location of the overall sailcraft, $\boldsymbol{m}_m$, by

$$\boldsymbol{m}_m = \boldsymbol{m} - \boldsymbol{r}_m^t\times\boldsymbol{f} \quad (21)$$

This $\boldsymbol{m}_m$ will be used for analyses of the attitude dynamics of the sailcraft.

Comparison of Results for Prescribed-Shape Sail

Based on the preceding formulation, a four-node quadrilateral membrane element that accounts for solar-pressure effect was implanted into the geometrically nonlinear FE code used in [10,12], which is written in MATLAB.[§] To demonstrate the adequacy of the FE formulation presented herein, FE results are presented subsequently that correspond to the analytical result of Rios-Reyes and Scheeres [8]. This comparison with the analytical result demonstrates the validity of the FE equations presented in Eqs. (14) and (16). For this special case, the sail shape is prescribed; in other words, the normal vector $\hat{\boldsymbol{n}}$ is given in terms of the sail geometries and coordinates. For a prescribed sail shape, the general analytical solution is obtained as follows, according to [8]. First, integration of Eq. (4) yields the analytical result

$$\boldsymbol{f} = P(r_s)[(a_1 - a_3)\beta\hat{\boldsymbol{r}}_0 \cdot \boldsymbol{J}^{(3)} \cdot \hat{\boldsymbol{r}}_0 + a_2\boldsymbol{J}^{(2)} \cdot \hat{\boldsymbol{r}}_0 + a_3\beta(\boldsymbol{J}^{(1)} \cdot \hat{\boldsymbol{r}}_0)\hat{\boldsymbol{r}}_0] \tag{22}$$

where $\boldsymbol{J}^{(3)} = \int_A \hat{\boldsymbol{n}}\,\hat{\boldsymbol{n}}\,\hat{\boldsymbol{n}}\,\mathrm{d}A$, $\boldsymbol{J}^{(2)} = \int_A \hat{\boldsymbol{n}}\,\hat{\boldsymbol{n}}\,\mathrm{d}A$, and $\boldsymbol{J}^{(1)} = \int_A \hat{\boldsymbol{n}}\,\mathrm{d}A$. The expression $\hat{\boldsymbol{n}}\,\hat{\boldsymbol{n}}$ represents an outer product, that is equivalent to $\hat{\boldsymbol{n}}\hat{\boldsymbol{n}}^T$ or $\hat{\boldsymbol{n}} \otimes \hat{\boldsymbol{n}}$. In obtaining Eq. (22), the relation $(\hat{\boldsymbol{n}} \cdot \hat{\boldsymbol{r}}_0)\hat{\boldsymbol{n}} = (\hat{\boldsymbol{n}}\,\hat{\boldsymbol{n}})\hat{\boldsymbol{r}}_0$ was used. Likewise, the corresponding analytical expression for the moment about the coordinate frame is given by

$$\boldsymbol{m} = P(r_s)[(a_1 - a_3)\beta\boldsymbol{K}^{(3)} \cdot \hat{\boldsymbol{r}}_0 + a_2\boldsymbol{K}^{(2)} \cdot \hat{\boldsymbol{r}}_0 + a_3\beta\boldsymbol{K}^{(1)} \cdot \tilde{\hat{\boldsymbol{r}}}_0] \tag{23}$$

where $\boldsymbol{K}^{(3)} = \int_A \tilde{\boldsymbol{x}} \cdot \hat{\boldsymbol{r}}_0 \cdot (\hat{\boldsymbol{n}}\,\hat{\boldsymbol{n}}\,\hat{\boldsymbol{n}})\,\mathrm{d}A$, $\boldsymbol{K}^{(2)} = \int_A \tilde{\boldsymbol{x}} \cdot (\hat{\boldsymbol{n}}\,\hat{\boldsymbol{n}})\,\mathrm{d}A$, and $\boldsymbol{K}^{(1)} = \int_A (\hat{\boldsymbol{n}} \cdot \hat{\boldsymbol{r}}_0)\boldsymbol{x}\,\mathrm{d}A$. The operator [~] forms a skew-symmetric matrix as shown in Appendix A. Equation (23) corrects an algebraic error that appears in Eq. (38) of [8]. Notice that $\boldsymbol{K}^{(3)}$ and $\boldsymbol{K}^{(1)}$ depend on the sun–photon incidence vector $\boldsymbol{r}_0$.

To compare the analytical results described by Eqs. (22) and (23) with the corresponding FE results obtained from Eqs. (14) and (16), an FE model of the billowed circular membrane presented in [8] was constructed as Fig. 3 illustrates. Figure 3 shows the model with 276 elements, and three other models with a different number of elements were also constructed for a convergence study. The billowed sail shape is given by the coordinates $y_3 = -[\gamma/(2R)](y_1^2 + y_2^2) + \gamma R/2$ for $y_1^2 + y_2^2 \le R^2$. Likewise, the normal vector is given by

$$\hat{\boldsymbol{n}} = \frac{1}{\sqrt{1 + (\gamma/R)^2 y_1^2 + (\gamma/R)^2 y_2^2}} \begin{bmatrix} (\gamma/R)y_1 \\ (\gamma/R)y_2 \\ 1 \end{bmatrix} \tag{24}$$

For this particular sail shape, the components of the tensors appearing in Eqs. (22) and (23) are given as follows:

$$J_3^{(1)} = \pi R^2$$

$$J_{11}^{(2)} = J_{22}^{(2)} = \pi R^2[2 + (\gamma^2 - 2)\sqrt{1 + \gamma^2}]/(3\gamma^2)$$

$$J_{33}^{(2)} = 2\pi R^2[\sqrt{1 + \gamma^2} - 1]/\gamma^2$$

$$J_{311}^{(3)} = J_{131}^{(3)} = J_{322}^{(3)} = J_{232}^{(3)} = J_{113}^{(3)} = J_{223}^{(3)} = \pi R^2[\gamma^2 - \ell_n(1 + \gamma^2)]/(2\gamma^2)$$

$$J_{333}^{(3)} = [\pi R^2\,\ell_n(1 + \gamma^2)]/\gamma^2$$

[§]Data available online at http://www.mathworks.com [cited 10 November 2006].

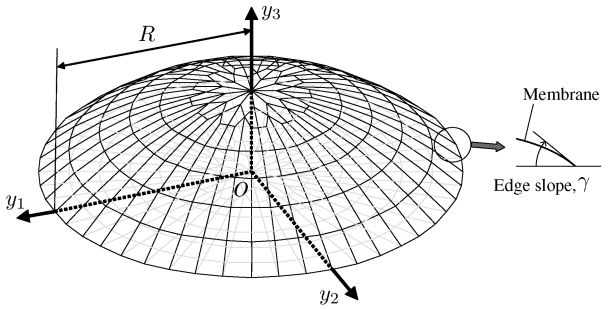

Fig. 3 Finite element model of billowed circular sail (with 276 elements).

$$K_1^{(1)} = (\gamma\pi R^3 \sin\alpha_0)/4$$

$$K_3^{(1)} = (\gamma\pi R^3 \cos\alpha_0)/4$$

$$K_{12}^{(2)} = -K_{21}^{(2)} = \pi R^3[6 - 5\gamma^2 - (6 - 8\gamma^2 + \gamma^4)\sqrt{1 + \gamma^2}]/(15\gamma^3)$$

$$K_{12}^{(3)} = -K_{21}^{(3)} = \pi R^3 \cos\alpha_0[\gamma^2(2 - \gamma^2) + 2(\gamma^2 - 1)\,\ell_n(1 + \gamma^2)]/(8\gamma^3)$$

$$K_{23}^{(3)} = \pi R^3 \sin\alpha_0[\gamma^2(\gamma^2 - 2) + 2(1 - \gamma^2)\,\ell_n(1 + \gamma^2)]/(8\gamma^3)$$

These equations show only the nonzero components of $\boldsymbol{J}^{(1)}$, $\boldsymbol{J}^{(2)}$, $\boldsymbol{J}^{(3)}$, $\boldsymbol{K}^{(1)}$, $\boldsymbol{K}^{(2)}$, and $\boldsymbol{K}^{(3)}$; thus, all the other components that do not appear are zero. To obtain expressions for $\boldsymbol{K}^{(3)}$ and $\boldsymbol{K}^{(1)}$, the sun–photon incidence vector must be prescribed. For the purpose of the present study,

$$\boldsymbol{r}_0 = \begin{bmatrix} \sin\alpha_0 & 0 & \cos\alpha_0 \end{bmatrix}^T$$

is used. The expressions $J_{11}^{(2)}$ and $J_{22}^{(2)}$ given in the preceding equations correct another error in [8].

For numerical comparison, the following values are used. The sail radius for this example is $R = 40$ m and the edge slope $\gamma = 1$ deg. In addition, the following optical coefficients for a nonideal sail are used, following [6]: $(\rho, s, e_f, e_b, B_f, B_b) = (0.88, 0.94, 0.05, 0.55, 0.79, 0.55)$. The sun distance $r_s = 0.3$ AU and the pitch angle $\alpha_0 = 45$ deg are also used. The analytical solutions with these parameters are shown in Table 1, and the errors of the corresponding FE results from the analytical solutions are presented in Fig. 4. Because of the symmetry of the problem and the definition of κ in Eq. (17),

$$\boldsymbol{m} = \begin{bmatrix} 0 & m_2 & 0 \end{bmatrix}^T$$

and

$$\boldsymbol{r}_p = \begin{bmatrix} r_{p1} & 0 & 0 \end{bmatrix}^T$$

thus, only m_2 and r_{p1} are presented here. Note that all values are measured from the coordinate origin. The number of elements is varied from 92 to 8262. As is seen in Fig. 4, the FE results monotonically converge to the analytical solutions. With 8262 elements, all the errors are less than 0.05%. This convergence

Table 1 Analytical solutions [Eqs. (22) and (23)] for a billowed circular sail with radius $R = 40$ m and edge slope $\gamma = 1$ deg

Optically nonideal sail, $r_s = 0.3$ AU and $\alpha_0 = 45$ deg	
Category	Value
Total force $\|\boldsymbol{f}\|$	2.32×10^{-1} N
Centerline angle ϕ	5.46 deg
Moment about origin m_2	-7.32×10^{-2} N · m
Center-of-pressure location r_{p1}	3.17×10^{-1} m

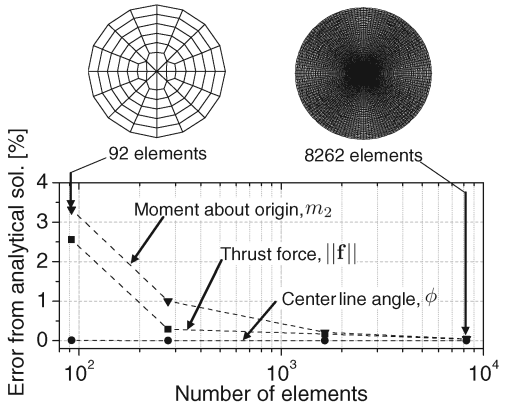

Fig. 4 Errors in finite element results from the analytical solutions.

suggests that the FE formulations presented in Eqs. (14) and (16) represent the physics well, thereby forces/torques in other sail configurations should be also accurately predicted by using the presented FE equations, if the FE meshes are sufficiently fine.

Comparisons for Solar and Gas-Pressure Loadings

Simplification of FE Equations

Though the analysis presented previously prescribes the sail curvature, this section considers the sail deformation in equilibrium with solar pressure. Notice that the solar-radiation force equation, Eq. (4), can be significantly simplified if the following two assumptions are made: $\hat{\boldsymbol{n}} \cdot \hat{\boldsymbol{r}}_0 \approx \hat{\boldsymbol{n}}_0 \cdot \hat{\boldsymbol{r}}_0$ and $\hat{\boldsymbol{r}}_0 - (\hat{\boldsymbol{n}} \cdot \hat{\boldsymbol{r}}_0)\hat{\boldsymbol{n}} \approx 0$, where $\hat{\boldsymbol{n}}_0$ is the unit normal vector of the undeformed sail reference surface. The first assumption implies that the change of the sun–photon incidence angle due to the membrane deformation can be ignored, that is, $(\alpha - \alpha_0) \approx 0$. This assumption is true when the deflection of the sail is very small. The second assumption implies that the tangential component of the solar pressure to the surface normal can be neglected. This assumption is usually justified for most realistic sails, because the tangential pressure component is typically less than 10% of the normal component for sun–photon incidence angles $\alpha < 45$ deg. For example, Eq. (1) becomes $\mathrm{d}\boldsymbol{f} = P(r_s)(0.906\hat{\boldsymbol{n}} + 0.086\hat{\boldsymbol{t}})\,\mathrm{d}A$ for the optically nonideal sail properties and $\alpha = \alpha_0 = 45$ deg. In addition, the in-plane fundamental natural frequency of the sail is usually much higher than the out-of-plane fundamental natural frequency; therefore, the in-plane displacement of the sail is less significant than the out-of-plane deflection.

When the two assumptions discussed in the preceding paragraph are applicable, the FE equations for the solar-pressure loading, Eqs. (8) and (A1) [used in Eq. (12)], are simplified to the FE equations for a uniform gas-pressure loading as follows:

$$\boldsymbol{p}\,(\xi_1, \xi_2) = \lambda P(r_s)\boldsymbol{n} \tag{25}$$

$$\frac{\partial \boldsymbol{p}}{\partial \boldsymbol{x}_i} = \lambda P(r_s)\frac{\partial \boldsymbol{n}}{\partial \boldsymbol{x}_i} \tag{26}$$

where

$$\lambda = \hat{\boldsymbol{n}}_0 \cdot \hat{\boldsymbol{r}}_0(a_1|\hat{\boldsymbol{n}}_0 \cdot \hat{\boldsymbol{r}}_0| + a_2) \tag{27}$$

$$= a_1\cos^2\alpha_0 + a_2\cos\alpha_0 \tag{28}$$

is a scale factor that is used to determine gas pressure corresponding to a given solar pressure. For an initially flat sail, the sun–photon incidence angle α_0 in Eq. (28) is constant throughout the sail; thus, λ is constant as well. On the other hand, for an initially curved surface, α_0 varies; thus, the vector expression in Eq. (27) will be more convenient for FE integration.

An FE model for gas-pressure loading can be validated using closed-form analytical solutions for simple membrane configurations, whereas such solutions cannot be obtained for solar-pressure loading. Hence, in the following subsections, the FE model for gas-pressure loading is first validated by comparing it to the analytical solution. Then, FE results for solar-pressure loading are compared to the corresponding gas-pressure loading cases to show that the FE model developed here represents the physics well. In addition, it shows that for a realistic solar-pressure value, the uniform gas-pressure model can accurately simulate the membrane deformation under the action of solar-pressure loading.

Validation of FE Model for Uniform Gas-Pressure Loading

To demonstrate the adequacy of the simplified FE equations, Eqs. (25) and (26), an FE model for an infinite-width membrane of length ℓ with two fixed edges, a uniform biaxial prestrain ε_0, and subjected to uniform gas-pressure load p was analyzed (see Fig. 5a). For this special configuration, the closed-form solution is given in Appendix B.

To compare the analytical solution with the corresponding FE results, the specific case with a length of $\ell = 80$ m, a width of 0.8 m, and the membrane properties given in Table 2 was considered. The FE model, shown in Fig. 5a, consists of 100 uniformly spaced four-node quadrilateral elements. All three displacements were constrained at the two supported edges, and the y_2-displacement along the free edges were constrained to simulate the deformation associated with the applied uniform gas pressure p. A comparison of the deformed shape obtained from the analytical solution and the corresponding FE model for a gas pressure $p = 1$ Pa is presented in Fig. 6. These results exhibit an excellent correlation with a maximum difference of 0.01%. This excellent agreement suggests that the FE equations are sufficient for predicting the deformation for this case.

Comparisons for Solar and Gas-Pressure Loadings

Next, the deformations of the same infinite-width membrane under solar pressure and gas pressure were compared to observe the physics of solar-radiation pressure and to show the adequacy of the

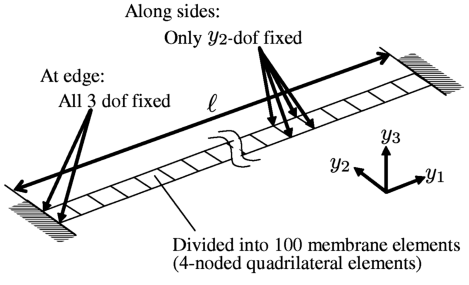

a) Finite element model

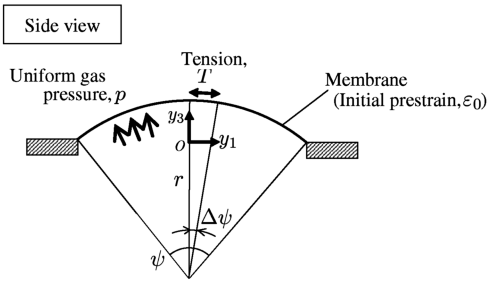

b) Deformed membrane cross section and nomenclature

Fig. 5 Two-edge fixed infinite-width membrane model subjected to solar/gas pressure.

Table 2 Material properties of sail membrane

Category	Value
Young's modulus E_m	3.454 GPa
Thickness h_m	5 μm
Poisson's ratio ν	0.312
Density ρ_m	1.44 g/cm^3
Prestrain ε_0	2μ-strain
(Corresponds to prestress $\sigma_m = 10$ kPa)	

simplified FE model. First, the solar pressure $P(r_s)$ was set at 1 Pa, and the sun vector was selected as

$$\hat{\boldsymbol{r}}_0 = \begin{bmatrix} \sin\alpha_0 & 0 & \cos\alpha_0 \end{bmatrix}^T$$

with $\alpha_0 = 45$ deg. The same nonideal optical coefficients in the preceding section were used. The corresponding uniform gas pressure is determined by using the scale factor λ in Eq. (27), which accounts for the effect of the optical properties of the sail and the sun-incidence angle. A comparison of the FE results for the two loading cases is shown in Fig. 7. The results indicate that the deflection amplitudes of the two models correspond very well, and that the solar-pressure model produces a slightly asymmetric deformation. This displacement in the y_1-direction is caused by the change of the sun–photon incidence angle α subsequent to the sail deflection and by the tangential component of the solar-radiation pressure. This result suggests that the membrane finite element derived here represents the membrane behavior under the action of solar-radiation pressure very well.

The 1 Pa solar pressure used in the preceding example is not a realistic value and was simply used to exaggerate the asymmetric deformation. A more practical solar pressure value used in the following is $P(r_s) = 5.0667 \times 10^{-5}$ Pa, which corresponds to the solar distance $r_s = 0.3$ AU. A comparison of the FE results for the infinite-width membrane subjected to this practical value of the solar pressure and the corresponding uniform gas pressure is presented in Fig. 8. For this practical solar pressure value, the deformations produced by the two loadings are almost identical. The maximum difference is approximately 0.5%. These results show that a scaled uniform gas-pressure loading can be used to obtain the deformed shape of a solar sail subjected to a realistic solar pressure. This result is significantly useful, because the FE model for gas pressure is easily constructed using commercially available geometrically nonlinear FEM software.

Finally, once the deformed shapes are determined from the FE analyses, Eqs. (14) and (16) are used to obtain the total force and torque exerted on the membrane sail. The results presented in the preceding section for the prescribed sail shape suggest that these equations should yield very accurate values for an accurately predicted deformed sail shape. The forces and moments calculated using the previously obtained deformed shapes, predicted for the realistic solar pressure and the corresponding uniform gas pressure, are presented in Table 3. The same parameters are used as in the preceding analyses. The cp location and the sail's cm location are also displayed. These results indicate that all the corresponding values for two loading conditions precisely agree.

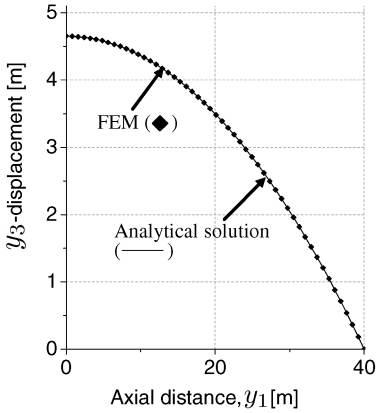

Fig. 6 Comparison between analytical solution and FE results for a uniform gas-pressure loading, $p = 1$ Pa.

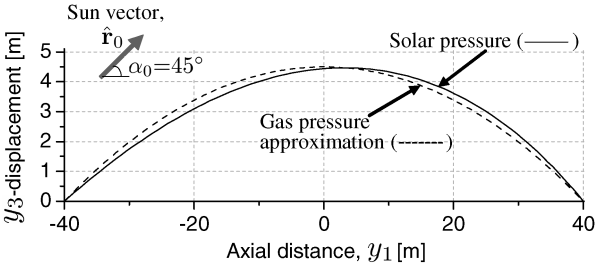

Fig. 7 Transverse displacement of the infinite-width membrane under solar/gas pressure ($P = 1$ Pa).

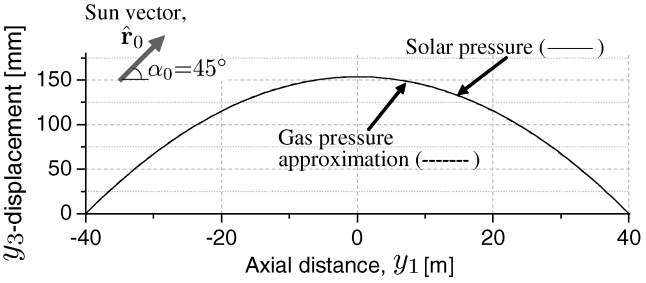

Fig. 8 Transverse displacement of the infinite-width membrane under solar/gas pressure [P(0.3 AU) = 5.0667 × 10^{-5} Pa].

Discussion

In the present study, two kinds of FE analyses were carried out. The first analysis verified the FE equations to compute the force and torque exerted on a billowed sail (step 1). This verification was accomplished by comparing the FE result to the analytical solution of Rios-Reyes and Scheeres [8]. The second analysis yielded the membrane deformation caused by solar pressure, predicted by the finite element developed herein, and the results were compared with

Table 3 Solar pressure effects on a solar-pressure model and a gas-pressure approximation model (membrane length $\ell = 80$ m, width 0.8 m, and prestrain $\varepsilon_0 = 2\mu$-strain)

Optically nonideal sail, sun distance $r_s = 0.3$ AU, and pitch angle $\alpha_0 = 45$ deg	Solar-pressure model	Gas approximation
Total force $\|\boldsymbol{f}\|$	2.95×10^{-3} N	2.95×10^{-3} N
Centerline angle ϕ	5.45 deg	5.45 deg
Moment about origin m_2	-5.47×10^{-4} N · m	-5.47×10^{-4} N · m
Center-of-pressure location r_{p1}	1.86×10^{-1} m	1.86×10^{-1} m
Center-of-mass deviation from origin $\|\boldsymbol{r}_{\text{cm}}\|$	1.03×10^{-1} m	1.03×10^{-1} m

a well-validated gas-pressure FE model. In particular, the analysis exhibited a physically valid result (step 2), and additionally, it found that the membrane deformation caused by solar pressure is accurately computed by using the corresponding uniform gas-pressure loading for a realistic solar pressure value. These results suggest that the FE model presented in this study represents the physics well, and thus, it can be used to model other solar-sail geometries. By using the FE model, an arbitrarily shaped sail, even with nonuniform prestress distributions, can be simulated, which is unattainable by analytical models.

This study has found a scaling factor λ in Eq. (27), which determines what gas pressure will approximately replace a given solar pressure for a sail with variable optical coefficients and a variable sun-incidence angle. As a result, the force and moment vectors, as well as the center of pressure location, can be computed accurately using any geometrically nonlinear FE software by the following three steps:

1) Determine the deformed sail shape using the scaled uniform gas pressure.

2) Compute the solar-radiation force vector for each element in the deformed configuration using Eqs. (5–10).

3) Sum the elemental force vectors to obtain the total force and moment exerted on the entire sail using Eqs. (14) and (16).

Conclusions

Starting with an optical solar-sail force model, a membrane finite element that can compute a deformed sail shape, caused by solar pressure, and that can obtain the total force and moment vectors exerted on the deformed sail has been developed. This special purpose finite element can also be used for transient dynamic analyses, and can include the effect of wrinkles by using tension-field theory. In addition, it has been shown that the finite element developed herein for solar-pressure loading can be simplified to a corresponding one for uniform gas-pressure loading, and a scale factor that relates two loading cases has been identified. The analysis results presented herein suggest that this gas-pressure loading model can be used to accurately simulate the sail deformation caused by solar-pressure loading when the change of the sun–photon incidence angle due to the sail deflection can be ignored and the effect of tangential component of the solar pressure can be neglected. This finding will significantly facilitate sailcraft analyses, through the use of commercial finite element codes, that will improve attitude controller design as well as structural design of sailcraft.

Appendix A: Jacobian of Solar-Radiation Force Vector

The expression $[\partial \boldsymbol{p}(\xi_1, \xi_2)/\partial \boldsymbol{x}_i]$ in Eq. (12) can be expanded, using the definition of $\boldsymbol{p}$ in Eq. (8), as

$$\frac{\partial \boldsymbol{p}}{\partial \boldsymbol{x}_i} = P(r_s)\Bigg\langle \{[(a_1 - a_3)\hat{\boldsymbol{n}} \cdot \hat{\boldsymbol{r}}_0 + a_2\beta]\hat{\boldsymbol{n}} + a_3\hat{\boldsymbol{r}}_0\}\left[\frac{\partial |\boldsymbol{n} \cdot \hat{\boldsymbol{r}}_0|}{\partial \boldsymbol{x}_i}\right] + |\boldsymbol{n} \cdot \hat{\boldsymbol{r}}_0|\left\{(a_1 - a_3)\hat{\boldsymbol{n}}\left[\frac{\partial (\hat{\boldsymbol{n}} \cdot \hat{\boldsymbol{r}}_0)}{\partial \boldsymbol{x}_i}\right] + [(a_1 - a_3)\hat{\boldsymbol{n}} \cdot \hat{\boldsymbol{r}}_0 + a_2\beta]\frac{\partial \hat{\boldsymbol{n}}}{\partial \boldsymbol{x}_i}\right\}\Bigg\rangle \tag{A1}$$

where

$$\frac{\partial (\hat{\boldsymbol{n}} \cdot \hat{\boldsymbol{r}}_0)}{\partial \boldsymbol{x}_i} = \hat{\boldsymbol{r}}_0^T\left[\frac{\partial \hat{\boldsymbol{n}}}{\partial \boldsymbol{x}_i}\right], \qquad \frac{\partial |\boldsymbol{n} \cdot \hat{\boldsymbol{r}}_0|}{\partial \boldsymbol{x}_i} = \operatorname{sgn}(\boldsymbol{n} \cdot \hat{\boldsymbol{r}}_0)\hat{\boldsymbol{r}}_0^T\left[\frac{\partial \boldsymbol{n}}{\partial \boldsymbol{x}_i}\right]$$

with

$$\frac{\partial \boldsymbol{n}}{\partial \boldsymbol{x}_i} = \frac{\partial (\boldsymbol{g}_1 \times \boldsymbol{g}_2)}{\partial \boldsymbol{x}_i} = \tilde{\boldsymbol{g}}_1\frac{\partial \boldsymbol{g}_2}{\partial \boldsymbol{x}_i} - \tilde{\boldsymbol{g}}_2\frac{\partial \boldsymbol{g}_1}{\partial \boldsymbol{x}_i}$$

$$\frac{\partial \hat{\boldsymbol{n}}}{\partial \boldsymbol{x}_i} = \frac{\partial}{\partial \boldsymbol{x}_i}\left[\frac{\boldsymbol{n}}{\|\boldsymbol{n}\|}\right] = \frac{1}{\|\boldsymbol{n}\|}\left(\frac{\partial \boldsymbol{n}}{\partial \boldsymbol{x}_i} - \hat{\boldsymbol{n}}\left[\frac{\partial \|\boldsymbol{n}\|}{\partial \boldsymbol{x}_i}\right]\right)$$

$$\frac{\partial \|\boldsymbol{n}\|}{\partial \boldsymbol{x}_i} = \frac{\partial \sqrt{\boldsymbol{n}^T\boldsymbol{n}}}{\partial \boldsymbol{x}_i} = \frac{1}{2\sqrt{\boldsymbol{n}^T\boldsymbol{n}}}2\boldsymbol{n}^T\left[\frac{\partial \boldsymbol{n}}{\partial \boldsymbol{x}_i}\right] = \frac{1}{\|\boldsymbol{n}\|}\boldsymbol{n}^T\left[\frac{\partial \boldsymbol{n}}{\partial \boldsymbol{x}_i}\right]$$

$$\frac{\partial \boldsymbol{g}_\alpha}{\partial \boldsymbol{x}_i} = \frac{\partial N_i}{\partial \xi_\alpha}\boldsymbol{I}$$

The quantity $[\partial P(r_s)/\partial \boldsymbol{x}_i] \approx \boldsymbol{0}$ is assumed, and $(\partial \boldsymbol{r}_0/\partial \boldsymbol{x}_i) = \boldsymbol{0}$ is used. The operator $[\tilde{}\,]$ forms a skew-symmetric matrix as follows:

$$\tilde{\boldsymbol{b}} = \begin{bmatrix} 0 & -b_3 & b_2 \\ b_3 & 0 & -b_1 \\ -b_2 & b_1 & 0 \end{bmatrix} \quad \forall\ \boldsymbol{b} = \begin{bmatrix} b_1 & b_2 & b_3 \end{bmatrix}^T \tag{A2}$$

Appendix B: Analytical Solution for the Infinite-Width Membrane Subjected to Uniform Gas-Pressure Load

An analytical solution for the infinite-width membrane subjected to uniform gas-pressure load (see Fig. 5a) is derived in this Appendix. Although some researchers discuss analytical solutions for membrane deformations subjected to uniform gas-pressure load with simple membrane geometries [13,14], they are mostly series solutions; thus, the solutions are difficult to handle and their accuracy is uncertain because their higher-order terms are normally neglected. On the other hand, the analytical solution presented here is a closed form, thus it is simple and accurate. Hence, it is suitable to be used for the validation of numerical models.

The analytical solution for this special case is obtained by presuming that the membrane deforms into a circular arc with radius r, as depicted in Fig. 5b. The equilibrium condition for the arc segment of the deformed membrane subtended by the small central angle $\Delta\psi$ of the deformed membrane, shown in Fig. 5b, is given by $2T\sin(\Delta\psi/2) = rp\Delta\psi$. Therefore, the membrane tension force per unit width is given by

$$T = rp \tag{B1}$$

For a general case, Green's strain tensor is defined in terms of displacements in each axis as (e.g., see [15])

$$e_{ij} = \frac{1}{2}\left(\frac{\partial u_j}{\partial y_i} + \frac{\partial u_i}{\partial y_j} + \frac{\partial u_\alpha}{\partial y_i}\frac{\partial u_\alpha}{\partial y_j}\right) \tag{B2}$$

For the current particular problem, $(\partial u_1/\partial y_1) = \varepsilon$ and $(\partial u_2/\partial y_2) = \varepsilon_0$ where $\varepsilon = \varepsilon_d + \varepsilon_0$ is the nominal strain in the y_1-direction of the deformed membrane, with $\varepsilon_d = (r\psi - \ell)/\ell_0$ and $\ell_0 = \ell/(1 + \varepsilon_0)$. Geometrically, $\sin(\psi/2) = \ell/(2r)$; thus, $\psi = 2\arcsin[\ell/(2r)]$. Consequently, the diagonal components of the strain tensor are given by

$$e_{11} = \varepsilon\left(1 + \frac{\varepsilon}{2}\right) \tag{B3}$$

$$e_{22} = \varepsilon_0\left(1 + \frac{\varepsilon_0}{2}\right) \tag{B4}$$

Using the generalized Hook's law, the normal stress in the y_1-direction, σ_{11}, is related to the strain components as

$$\sigma_{11} = \frac{E_m}{1 - \nu^2}(e_{11} + \nu e_{22}) \tag{B5}$$

From the principle of virtual work, the virtual work by the tension in the y_1-direction per unit width applied to an infinitesimal volume of the membrane $\mathrm{d}V = h_m\,\mathrm{d}y_1$ is expressed as

$$T\delta u_1 = \int_V \sigma_{11}\delta e_{11}\,\mathrm{d}V \tag{B6}$$

$$= \sigma_{11}\delta e_{11}(h_m\,\mathrm{d}y_1) \tag{B7}$$

where $\delta[\,]$ represents a variation. Because $\delta u_1 = \mathrm{d}y_1\delta\varepsilon$ and $\delta e_{11} = (1+\varepsilon)\delta\varepsilon$ [from Eq. (B3)], Eq. (B7) becomes

$$T = h_m\sigma_{11}(1+\varepsilon) \tag{B8}$$

The substitution of Eqs. (B3–B5) into Eq. (B8) gives the tension force per unit width of the membrane in terms of the nominal strains as

$$T = \frac{E_m h_m}{1-\nu^2}\left[\varepsilon\left(1+\frac{\varepsilon}{2}\right) + \nu\varepsilon_0\left(1+\frac{\varepsilon_0}{2}\right)\right](1+\varepsilon) \tag{B9}$$

Note that ε, the nominal strain in the y_1-direction, is a function of the radius of deformed membrane, r. By using Eq. (B9), Eq. (B1) is solved numerically for r. Once r is obtained, the deformed membrane shape is given by

$$y_3 = \sqrt{r^2 - y_1^2} - \sqrt{r^2 - \frac{\ell^2}{4}}, \qquad -\frac{\ell}{2} \le y_1 \le \frac{\ell}{2} \tag{B10}$$

Acknowledgment

H. Sakamoto is supported by Japan Society for the Promotion of Science (JSPS) Postdoctoral Fellowships for Research Abroad 2005.

References

[1] Mettler, E., and Ploen, S. R., "Solar Sail Dynamics and Control Using a Boom Mounted Bus Articulated by a Bi-State Two-Axis Gimbal and Reaction Wheels," AIAA Paper 2002-4992, 2002.

[2] Wie, B., "Solar Sail Attitude Control and Dynamics, Part 2," *Journal of Guidance, Control, and Dynamics*, Vol. 27, No. 4, July–Aug. 2004, pp. 536–544.

[3] Wie, B., Murphy, D., Paluszek, M., and Thomas, S., "Robust Attitude Control Systems Design for Solar Sails, Part 1: Propellantless Primary ACS," AIAA Paper 2004-5010, 2004.

[4] Wie, B., "Solar Sail Attitude Control and Dynamics, Part 1," *Journal of Guidance, Control, and Dynamics*, Vol. 27, No. 4, July–Aug. 2004, pp. 526–535.

[5] Wright, J. L., *Space Sailing*, Gordon and Breach Science Publishers, Philadelphia, PA, 1992, Appendix B.

[6] McInnes, C. R., *Solar Sailing: Technology, Dynamics and Mission Applications*, Springer–Verlag, New York, 1999, Chap. 2.

[7] Mengali, G., and Quarta, A. A., "Optimal Three-Dimensional Interplanetary Rendezvous Using Nonideal Solar Sail," *Journal of Guidance, Control, and Dynamics*, Vol. 28, No. 1, Jan.–Feb. 2005, pp. 173–177.

[8] Rios-Reyes, L., and Scheeres, D. J., "Generalized Model for Solar Sails," *Journal of Spacecraft and Rockets*, Vol. 42, No. 1, Jan.–Feb. 2005, pp. 182–185.

[9] Salama, M., White, C., and Leland, R., "Ground Demonstration of a Spinning Solar Sail Deployment Concept," *Journal of Spacecraft and Rockets*, Vol. 40, No. 1, Jan.–Feb. 2004, pp. 9–14.

[10] Miyazaki, Y., "Wrinkle/Slack Model and Finite Element Dynamics of Membrane," *International Journal for Numerical Methods in Engineering*, Vol. 66, No. 7, May 2006, pp. 1179–1209.

[11] Miyazaki, Y., and Uchiki, M., "Deployment Dynamics of Inflatable Tube," AIAA Paper 2002-1254, 2002.

[12] Sakamoto, H., Park, K. C., and Miyazaki, Y., "Dynamic Wrinkle Reduction Strategies for Cable Suspended Membrane Structures," *Journal of Spacecraft and Rockets*, Vol. 42, No. 5, Sept.–Oct. 2005, pp. 850–858.

[13] Campbell, J. D., "On the Theory of Initially Tensioned Circular Membrane Subjected to Uniform Pressure," *Quarterly Journal of Mechanics and Applied Mathematics*, Vol. 9, No. 1, 1956, pp. 84–93.

[14] Fichter, W. B., "Some Solutions for the Large Deflections of Uniformly Loaded Circular Membranes," NASA TP-3658, July 1997.

[15] Fung, Y. C., and Tong, P., *Classical and Computational Solid Mechanics*, World Scientific, Farrer Road, Singapore, 2001, Chap. 4.

M. Nemeth
Associate Editor